RAIRO-Oper. Res. 56 (2022) 3047–3069
https://doi.org/10.1051/ro/2022137

RAIRO Operations Research
www.rairo-ro.org

AN IMPROVED PDE-CONSTRAINED OPTIMIZATION FLUID REGISTRATION FOR IMAGE MULTI-FRAME SUPER RESOLUTION

Amine Laghrib[1], Aissam Hadri[2,*], Moad Hakim[3] and Hssaine Oummi[1]

Abstract. The main idea of multi-frame super resolution (SR) algorithms is to recover a single high-resolution image from a sequence of low resolution ones of the same object. The success of the SR approaches is often related to a well registration and restoration steps. Therefore, we propose a new approach based on a partial differential equation (PDE)-constrained optimization fluid image registration and we use a fourth order PDE to treat both the registration and restoration steps that guarantee the success of SR algorithms. Since the registration step is usually a variational ill-posed model, a mathematical study is needed to check the existence of the solution to the regularized problem. Thus, we prove the existence and of the well posed fluid image registration and assure also the existence of the used second order PDE in the restoration step. The results show that the proposed method is competitive with the existing methods.

Mathematics Subject Classification. 49-XX, 49MXX, 49M41.

Received December 27, 2021. Accepted July 31, 2022.

1. Introduction

Image super resolution represents an active research area in the imagery domain. The main principle of this method is to recover a high-resolution (HR) image through a single image (Single-image SR) [23,43,47], or using a serie of low-resolution (LR) ones that are down-sampled, ill-registered, blurred and usually noised (multi-frame SR) [13,27,50]. SR intervenes in numerous domains, such as video surveillance and medical diagnostics [18].

The multi-frame and single SR are both intensively studied in order to improve the resolution of an image. In single SR technique, the missing information in the LR image is estimated from a large number of training. Then its success depends on the availability of a convenient dictionary which is not ensured in large application areas. While for the multi-frame SR the success is related to the approximation accuracy of the motion between the LR images. Since multiframe SR is more complicated in the presence of different degradation operators, Sina Farsiu et al [15] proposed the fast robust super resolution (RSR). The aim of this new technique is to break down the SR method into two steps: looking for a degraded HR image from the estimated LR frames after a registration procedure; then in a second step, restoring it [15].

Keywords. Super resolution, bilevel PDE, fluid registration, image restoration, regularization.

[1] EMI FST Béni-Mellal, Université Sultan Moulay Slimane, Maroc, North Africa
[2] LABSIV, Université Ibn Zohr, Maroc, North Africa
[3] Université Cadi Ayyad, LAMAI FST Marrakech, Maroc, North Africa.
*Corresponding author: aissamhadri20@gmail.com

On another side, nonlinear PDEs have also been treated in the super-resolution context with pleasant results. One of the consistent nonlinear PDEs was proposed by Maiseli *et al.* [35], which takes the advantages of Perona-Malik equation and the TV norm. This adaptive diffusion-based PDE can efficiently preserve image features but it suffers from the blurring effect. A more robust PDE was proposed by El Mourabit *et al.* [13, 14] which takes into consideration the coherence-enhancing property and avoids blur much better. However, when the blur and noise levels are too high, the obtained HR image still contains some artefacts, in particular the blur. More recently a fourth-order nonlinear PDE has been introduced with much more constrained diffusion that stops the edges destruction and preserve the smooth areas and texture [30]. In contrast, the blur apparition problem is still a remaining weakness of this PDE.

The first step of multiframe SR aim is to guess the motion between the LR frames to register all LR images in a common way [51]. This stage is the key of the success of multiframe SR algorithms and without a good estimation of the motion between the LR images, the super-resolution becomes very limited [7]. To overcome the difficulties of the registration step, many works have been proposed. These methods include the projection on a convex set (POCS) [46], the iterative back projection (IBP) [40], optical-flow [6]. However, these methods suffer from the non-uniqueness of solutions, and the fact that they consider only translational and rotational motion between the LR frames. More robust approaches are then proposed [41,50] to tackle the misregistration errors. One of the most successful methods was the nonlocal-means proposed by Protter *et al.* [39] which is applied to nonglobal motion. Otherwise, to treat nonparametric deformations between the LR images, an elastic registration was proposed in [26], but it is specified to small deformations and does not tackle larger ones. Other techniques use the maximum a posteriori (MAP) [2,17,38] with accurate spatial domain observation model to reconstruct the HR image. More recently, other methods were proposed [5] but still suffering from the misregistration errors.

In this paper, we follow the steps of the RSR method, while the registration approach and the second step are improved. Indeed, we propose a fluid image registration in a well-posed functional framework to handle the registration part of SR. In addition, to justify this choice, we show the existence and the uniqueness of the solution using classical mathematical approaches [9]. However, since the problems of deblurring and denoising are in most cases ill-posed, in the second step of SR, we have to obtain a related well-posed model based on regularization. Among the most-used regularization techniques, we have the Tikhonov-type functions [20, 47] and also Total Variation (TV) priors [19,28,35]. Meanwhile, second and fourth order PDE's have been proposed to avoid the staircasing effect, during the denoising process [8,11]. Recently, a Combined first and second-order approach has had a great success in denoising and deconvolution problems [37]. Thus, inspired by this work, we use the resulting fourth-order-Euler-Lagrange equation to remove noise and blur, this increases the robustness of the second step of the proposed SR algorithm.

This paper follows this configuration: Section 2 introduces the super resolution formulation. We introduce then the fluid registration and how to define the warp operators in Section 3. In Section 4, we describe briefly the proposed PDE and the main algorithm used in the deconvolution and denoising step. Finally, simulated and real results with comparisons of the proposed SR method to some available methods are presented in Section 5.

2. Problem formulation

In the presence of many degradation factors, the acquired images are always in a non desired resolution. In fact, the obtained images are decimated, noised and also blurred. We consider that the LR images are taken in the same conditions with one sensor. The link between the HR image X (described by a vector of size $[r^2N^2 \times 1]$ where r is the enhancement factor) and the associated low resolution frames Y_k (represented by a vector of size $[N^2 \times 1]$), is given by

$$Y_k = DF_kHX + e_k \qquad \forall k = 1, 2, \ldots, n, \tag{2.1}$$

where

H: the convolution operator describing the blur of size $[r^2N^2 \times r^2N^2]$.

D: the decimation operator which is related to the desired resolution of the HR image of size $[N^2 \times r^2N^2]$.
F_k: are the motions or the warp matrix of size $[r^2N^2 \times r^2N^2]$, representing random transformation between the LR frames.
e_k : is the additive Gaussian noise vector of size $[N^2 \times 1]$.

The aim of multi-frame super resolution is the recovery of an ideal HR image X. Due to the complexity of the problem we split it in two procedure [15]:

1. Approximating the transformation matrix F_k between each couple of LR images and merge the HR image B with noise and blur.
2. Computing the HR image X through the blurring and noisy one B.

We start by the approximation of the warp matrix F_k and also by ensuring the existence of the solution in a suitable functional space [1,9,12,27].

3. The construction of the warp matrix F_k

To construct the operators F_k, we use a fluid registration algorithm. This approach is based on the resolution of a variational minimization problem using fluid regularization term and an L^2 based data term to model the optical flow constraint. For that, we used bicubic upsampled $\widehat{Y}_i$ of the LR sequence Y_i. We then selected the reference image between the upsampled images $\widehat{Y}_i$ that is used for the super-resolution process as $\widehat{Y}_k$ $(1 \leq k \leq n)$. Through the image $\widehat{Y}_k$, we compute the optical flow to all other input images (for $i \neq k$). We then get n flow vector fields $u_i : \Omega \longrightarrow \mathbb{R}^2$. To simplify the notations we set $Y_k(x)$ the pixel value corresponding to the kth frame such as the coordinate $x = (x_1, x_2) \in \Omega \subset \mathbb{R}^2$ (Ω is the domain containing all the pixels). The image fluid registration problem is formulated as

$$Y(x) = Y_k(v_k(x)) \qquad \text{for } k = 2, \ldots, n \quad \text{and} \quad \forall x \in \Omega. \tag{3.1}$$

Our goal is to find the velocity deformation v_k that links each image to the reference one, where

$$v_k = \partial_t u_k + \nabla u_k . v_k, \tag{3.2}$$

∂_t is the partial time derivative operator and u_k are the deformations between each frame. Unfortunately, this problem is ill-posed. We have therefore to choose an appropriate regularization operator S. Since we know the success of the fluid registration to handle different problems in image registration [36], we propose to use it in a well-posed functional framework. The image fluid registration problem is defined as

$$\min_{u_k \in \mathcal{T} \text{ and } v_k \in \mathcal{U}_{ad}} \mathcal{J}(u_k, v_k), \tag{3.3}$$

where $\mathcal{J}(u_k, v_k) = \mathcal{D}(Y, Y_k, u_k) + \beta(S_1(u_k) + S_2(v_k))$, such that u_k is a solution of

$$\begin{cases} \partial_t u_k + \nabla u_k . v_k = 0, \ in \ \ \Omega \times (0,T), \\ u_k(x,t) = 0, \ on \ \ \partial\Omega \times (0,T), \\ u_k(x,0) = u_0, \ in \ \ \Omega \times (0,T), \end{cases} \tag{3.4}$$

where $\mathcal{T}$ represents the set of admissible transformations, while $\mathcal{U}_{ad}$ is the set of admissible velocity deformations, and β is the regularisation parameter.
$\mathcal{D}$: is the squared difference measure defined by Lebesgue L^2 norm as

$$\mathcal{D}(Y, Y_k, u_k) = \int_0^T \int_\Omega \left(Y_k(u_k(x,t)) - Y(x,t)\right)^2 \mathrm{d}x\mathrm{d}t, \tag{3.5}$$

the registration regularisation is given as follow

$$S_1(u_k) = \int_0^T \int_\Omega |\nabla u_k|^2 \mathrm{d}x\mathrm{d}t, \tag{3.6}$$

and the fluid regularisation is defined as

$$S_2(v_k) = \int_\Omega \mu \,(\mathrm{trace}V)^2 + \frac{\lambda}{2}\,\mathrm{trace}(V^2)\mathrm{d}x, \tag{3.7}$$

where V is the Cauchy strain tensor (for $||\nabla v_k|| \leq 1$) defined as $V(v_k) = (\nabla v_k + \nabla v_k)/2$, and μ and λ are the Lamé parameters. To ensure the existence of a unique solution to the problem (3.4), we have to choose firstly a functional framework. A natural choice of the functional space for every fixed $v_k \in \mathcal{U}_{ad}$ is

$$\begin{aligned}\mathcal{U}_{ad} = \big\{ & v \in (L^2((0,T)\times\Omega))^2 \text{ such that:} \\ & \|v\|_{(L^\infty(0,T;L^\infty(\Omega))^2} + \|v\|_{(L^2(0,T;H^1(\Omega))^2} + \|\partial_t v\|_{(L^2(((0,T)\times\Omega))^2} \leq C \\ & \text{and } div(v) = 0 \text{ .a.e in } \partial\Omega\big\}.\end{aligned} \tag{3.8}$$

For this reason, the existence of a unique solution is guaranteed in

$$\mathcal{T} = L^\infty(0,T;L^2(\Omega)), \tag{3.9}$$

which is presented in details in [32]. In the following, we present the main theorem of the existence of the solution to the proposed fluid image registration.

Theorem 3.1. *Let Ω be a regular bounded open subset of $\mathbb{R}^2$. The problem (3.3) admits at least a solution in $L^2(0,T;H_0^1(\Omega)) \times \mathcal{U}_{ad}$.*

Proof. Let $(u_{k,n}, v_{k,n})_n$ be a minimizing sequence of J such that $(u_{k,n}, v_{k,n})_n \in L^2(0,T,H_0^1(\Omega)) \times \mathcal{U}_{ad}$, and

$$\lim_{n\to\infty} J(u_{k,n}, v_{k,n}) = \inf_{(u_k,v_k)\in L^2(0,T,H^1(\Omega))\times\mathcal{U}_{ad}} J(u_k, v_k),$$

then we have

$$D(Y, Y_k, u_{k,n}) + \beta(S_1(u_{k,n}) + S_2(v_{k,n})) \leq C \tag{3.10}$$

which means

$$\|u_{k,n}\|^2_{L^2(0,T;H_0^1(\Omega))} \leq C, \tag{3.11}$$

we have to prove also that $\partial_t u_{k,n}$ is bounded. From equation (3.4), we get

$$|\int_0^T \int_\Omega \partial_t u_{k,n}\phi \mathrm{d}x\mathrm{d}t| \leq |\int_0^T \int_\Omega v_{k,n}\nabla u_{k,n}\phi \mathrm{d}x\mathrm{d}t|, \tag{3.12}$$

since $v_{k,n}$ is bounded in $\mathcal{U}_{ad} \subset (L^\infty((0,T)\times\Omega))^2$, then

$$|\int_0^T \int_\Omega \partial_t u_{k,n}\phi \mathrm{d}x\mathrm{d}t| \leq \|v_{k,n}\|_{(L^\infty(0,T;L^\infty(\Omega)))^2}\|\nabla u_{k,n}\|_{(L^2(0,T;L^2(\Omega)))^2}\|\phi\|_{L^2(0,T;L^2(\Omega))}. \tag{3.13}$$

we obtain

$$\|\partial_t u_{k,n}\|_{L^2(0,T;L^2(\Omega))} \leq C. \tag{3.14}$$

Now from the estimation (3.11) and estimation (3.14), we can extract a subsequence still denoted $(u_{k,n})_n$, such that:

$$u_{k,n} \rightharpoonup u_k^* \text{ in } L^2(0,T;H_0^1(\Omega)), \tag{3.15}$$

$$\partial_t u_{k,n} \rightharpoonup \partial_t u_k^* \text{ in } L^2(0,T;L^2(\Omega)). \tag{3.16}$$

We have also $\mathcal{U}_{ad}$ is compact in $(L^2(0,T;L^2(\Omega))$ by Aubin-Lions lemma [4], then we can extract a subsequence still denoted $(v_{k,n})_n$ such that

$$v_{k,n} \underset{n\to+\infty}{\longrightarrow} v_k^* \text{ in } (L^2(0,T;L^2(\Omega)))^2. \tag{3.17}$$

and

$$v_{k,n} \rightharpoonup v_k^* \text{ in } L^2(0,T;H^1(\Omega)), \tag{3.18}$$

We have to show the continuity of the solution for the direct problem, compared to the minimizing sequences $(u_{k,n}, v_{k,n})_n$. Which means we have to prove that (u_k^*, v_k^*) verifies the system (3.4). Let's prove that

$$\int_0^T \int_\Omega \partial_t u_{k,n}\phi \mathrm{d}x\mathrm{d}t \underset{n\to+\infty}{\longrightarrow} \int_0^T \int_\Omega \partial_t u_k^*\phi \mathrm{d}x\mathrm{d}t, \quad \forall \phi \in L^2(0,T;L^2(\Omega)), \tag{3.19}$$

and

$$\int_0^T \int_\Omega v_{k,n}\nabla u_{k,n}\phi \mathrm{d}x\mathrm{d}t \underset{n\to+\infty}{\longrightarrow} \int_0^T \int_\Omega v_k^*\nabla u_k^*\phi \mathrm{d}x\mathrm{d}t, \quad \forall \phi \in L^2(0,T;L^2(\Omega)). \tag{3.20}$$

For the convergence (3.19), it is obtained directly from (3.16). To show the convergence (3.20), we denote by

$$I = \int_0^T \int_\Omega (v_{k,n}\nabla u_{k,n} - v_k^*\nabla u_k^*)\phi \mathrm{d}x\mathrm{d}t, \quad \forall \phi \in L^2(0,T;L^2(\Omega)) = I_1 + I_2,$$

with

$$I_1 = \int_0^T \int_\Omega v_k^*(\nabla u_{k,n} - \nabla u_k^*)\phi \mathrm{d}x\mathrm{d}t, \quad \forall \phi \in L^2(0,T;L^2(\Omega)),$$

and

$$I_2 = \int_0^T \int_\Omega (v_{k,n} - v_k^*)\nabla u_{k,n}\phi \mathrm{d}x\mathrm{d}t, \quad \forall \phi \in L^2(0,T;L^2(\Omega)),$$

Let's prove that $I_i \underset{n\to+\infty}{\longrightarrow} 0$ for $i = 1, 2$. For the convergence of I_1, we have v_k^* in $(L^\infty((0,T)\times\Omega))^2$ and $\phi \in L^2(0,T;L^2(\Omega))$, which means that $v_k^*\phi$ in $(L^2(0,T;L^2(\Omega)))^2$. By using the convergence (3.15), we obtain that $I_1 \underset{n\to+\infty}{\longrightarrow} 0$. For I_2, by using Hölder inequality we have

$$|I_2| \leq [\int_0^T \int_\Omega ((v_{k,n} - v_k^*)\phi)^2 \mathrm{d}x\mathrm{d}t]^{\frac{1}{2}} \|\nabla u_{k,n}\|_{(L^2(0,T;L^2(\Omega)))^2} \leq C[\int_0^T \int_\Omega ((v_{k,n} - v_k^*)\phi)^2 \mathrm{d}x\mathrm{d}t]^{\frac{1}{2}}.$$

From the convergence (3.17), we have

$$v_{k,n} \underset{n\to+\infty}{\longrightarrow} v_k^* \text{ in } (L^2(0,T;L^2(\Omega)))^2,$$

which implies

$$v_{k,n} \underset{n\to+\infty}{\longrightarrow} v_k^* \text{ a.e. in } \Omega\times(0,T),$$

and using the fact that $v_{k,n}$ and v_k^* are bounded in $\mathcal{U}_{ad} \subset (L^\infty((0,T)\times\Omega))^2$, then

$$|(v_{k,n} - v_k^*)\phi|^2 \leq C|\phi|^2 \in L^1(\Omega\times(0,T)).$$

By applying the Lebesgue convergence, we obtain

$$[\int_0^T \int_\Omega ((v_{k,n} - v_k^*)\phi)^2 \mathrm{d}x\mathrm{d}t]^{\frac{1}{2}} \underset{n\to+\infty}{\longrightarrow} 0,$$

which means $I_2 \underset{n\to+\infty}{\longrightarrow} 0$.

Now we prove that the functional J is lower semi-continuous. For this, we have $u_{k,n} \underset{n\to+\infty}{\longrightarrow} u_k^*$ in $L^2(\Omega \times (0,T))$ and Y_k is continuous, then $\int_0^T \int_\Omega |Y_k(u_{k,n}) - Y|^2 \mathrm{d}x\mathrm{d}t \underset{n\to+\infty}{\longrightarrow} \int_0^T \int_\Omega |Y_k(u_k^*) - Y|^2 \mathrm{d}x\mathrm{d}t$. We have also the convergence (3.15) and the convergence (3.18), we obtain then

$$S_1(u_k^*) + S_2(v_k^*) \leq \liminf(S_1(u_{k,n}) + S_2(v_{k,n})).$$

which implies that $J(u_k^*, v_k^*) \leq \liminf J(u_{k,n}, v_{k,n})$. Thus

$$\lim_{n\to\infty} J(u_{k,n}, v_{k,n}) = \inf_{(u_k,v_k)\in\mathcal{U}_{ad}} J(u_k, v_k) = J(u_k^*, v_k^*).$$

Which concludes that the problem (3.3) admits at least a solution in $L^2((0,T), H_0^1(\Omega)) \times \mathcal{U}_{ad}$. □

To solve the minimisation problem (3.3), we use the BFGS algorithm [42]. For that, we have to obtain some optimality conditions on the functional $\mathcal{L}$.

4. Necessary Optimality conditions

In this section, we formally give the optimality conditions of the optimization problem, since we need them to compute the BFGS Algorithm. Before showing the optimality conditions, we give briefly in the following the gradient of S_2.

Proposition 4.1. *Let h_1 be a perturbation of v_k such that $v_k + h_1$ in $\mathcal{U}_{ad}$, then we have the following results*

$$dS_2(v_k).h_1 = -\int_0^T \int_\Omega \big(\mu\Delta v_k + (\mu+\lambda)\nabla div(v_k)\big).h_1 \ \mathrm{d}x\mathrm{d}t. \tag{4.1}$$

Proof. In the proof, we assume that $div(v_k) = (\nabla v_{k,i} + \partial_{x_i} v_k).n = 0 \quad in \quad \partial\Omega$. Then the derivative of S_2 with respect of v_k in direction h_1 is given by:

$$dS_2(v_k).h_1 = \lim_{r\to 0} \frac{S_2(v_k + rh_1) - S_2(v_k)}{r}$$

$$= \int_0^T \int_\Omega (\lambda+\mu) div(v_k) div(h_1) + \mu \sum_{i=1}^{2} \nabla v_{k,i} \nabla h_{1,i} \mathrm{d}x\mathrm{d}t$$

$$= -\int_0^T \int_\Omega (\lambda+\mu)\nabla div(v_k).h_1 + \mu \sum_{i=1}^{2} \Delta v_{k,i} h_{1,i} \mathrm{d}x\mathrm{d}t + \int_0^T \int_{\partial\Omega} (\lambda+\mu) div(v_k) h.n + \mu \sum_{i=1}^{2} h_{1,i} \nabla v_{k,i}.n \mathrm{d}x\mathrm{d}t,$$

$$= -\int_0^T \int_\Omega (\lambda+\mu)\nabla div(v_k).h_1 + \mu\Delta v_k.h_1 \mathrm{d}x\mathrm{d}t + \int_0^T \int_{\partial\Omega} \lambda div(v_k) h_1.n + \sum_{i=1}^{2} \mu h_{1,i} (\nabla v_{k,i} + \partial_{x_i} v_k).n \mathrm{d}x\mathrm{d}t,$$

since $div(v_k) = 0$ and $(\nabla v_{k,i} + \partial_{x_i} v_k).n = 0$ in $\partial\Omega$, we have:

$$dS_2(v_k).h = -\int_0^T \int_\Omega \big(\mu\Delta v_k + (\mu+\lambda)\nabla div(v_k)\big).h_1 \ \mathrm{d}x\mathrm{d}t.$$

□

Now we give the optimality conditions of the problem (3.3) in the following theorem.

Proposition 4.2. *Let v_k be a solution of the problem (3.3) with u_k its associated state and p_k a Lagrange multiplier, which are satisfying the following conditions:*

$$\begin{pmatrix} \partial_t u_k + v_k \nabla u_k \\ u_k(0,x) - u_0(x) \\ (Y(u_k) - Y_k(x))Y'(u_k) - \beta\Delta u_k - \partial_t p_k - div(v_k p_k) \\ p_k(T,x) \\ -\mu\Delta v_k - (\mu+\lambda)\nabla div(v_k) + \nabla u_k p_k \end{pmatrix} = \begin{pmatrix} 0 \\ 0 \\ 0 \\ 0 \\ 0 \end{pmatrix}.$$

Proof. In order to compute the optimality conditions, we must define first the Lagrangian function, which is given as follows:

$$\mathcal{L}(u_k, v_k, p_k) = D(Y, Y_k, u_k) + \beta S_1(u_k) + \beta S_2(v_k) + \int_0^T \int_\Omega (\partial_t u_k + v_k \nabla u_k) p_k \mathrm{d}x\mathrm{d}t,$$

where p_k is a Lagrange multiplier. We know from the theorem 3.1 that the problem (3.3) has at least one solution, this means that $\mathcal{L}$ admits u_k, v_k and p_k as saddle points, which give us the following iteration:

$$d_{v_k}\mathcal{L}(u_k, ., .).h_1 = 0, \quad d_{u_k}\mathcal{L}(., v_k, .).h_2 = 0 \text{ and } d_{p_k}\mathcal{L}(., ., p_k).h_3 = 0, \tag{4.2}$$

where h_i (for $i = 1, 2, 3$) are the derivative direction for each argument of $\mathcal{L}$. After developing derivation for each argument of the Lagrangian function and using the proposition above, we find

$$d_{v_k}\mathcal{L}(u_k, ., .).h_1 = -\int_0^T \int_\Omega \big(\mu\Delta v_k + (\mu+\lambda)\nabla div(v_k)\big).h_1 + h_1 \nabla u_k p_k \mathrm{d}x\mathrm{d}t = 0 \tag{4.3}$$

$$d_{u_k}\mathcal{L}(., v_k, .).h_2 = 2\int_0^T \int_\Omega ((Y(u_k) - Y_k(x))Y'(u_k) - \beta\Delta u_k)h_2 + (\partial_t h_2 + v_k \nabla h_2)p_k \mathrm{d}x\mathrm{d}t = 0, \tag{4.4}$$

and

$$d_{p_k}\mathcal{L}(., ., p_k).h_3 = \int_0^T \int_\Omega (\partial_t u_k + v_k \nabla u_k)h_3 \mathrm{d}x\mathrm{d}t = 0. \tag{4.5}$$

We can deduce the following

$$F(u_k, v_k, p_k) = \begin{pmatrix} \partial_t u_k + v_k \nabla u_k \\ u_k(0,x) - u_0(x) \\ (Y(u_k) - Y_k(x))Y'(u_k) - \beta\Delta u_k - \partial_t p_k - div(v_k p_k) \\ p_k(T,x) \\ -\mu\Delta v_k - (\mu+\lambda)\nabla div(v_k) + \nabla u_k p_k \end{pmatrix} = \begin{pmatrix} 0 \\ 0 \\ 0 \\ 0 \\ 0 \end{pmatrix}.$$

□

5. Algorithm details

We now give the details of each step of the BFGS Algorithm 1 described previously.

We will now explain in detail the implementation of the operators D, F_k and H. We begin by the downsampling operator D which transforms the $([r^2N^2 \times 1])$ HR image to the $([N^2 \times 1])$ LR sequence, where r is the decimation factor. For example, if $r = 2$, the decimation matrix D is given as follows

$$D = D_1 \otimes D_1, \tag{5.1}$$

Algorithm 1 The BFGS algorithm to compute u_k, v_k and p_k, respectively.

Require: Guess u_0, v_0 and p_0.

1. Set $k := 0$.
2. Evaluate $d_k := \eta_k := \begin{pmatrix} -d_{u_k}\mathcal{L}(u_k,.,.) \\ -d_{v_k}\mathcal{L}(.,u_k,.) \\ -d_{p_k}\mathcal{L}(.,.,p_k) \end{pmatrix} = \begin{pmatrix} d_k^1 \\ d_k^2 \\ d_k^3 \end{pmatrix}$
3. **While** stopping criteria are violated **do**
4. Obtain step length $t_k = (t_k^1, t_k^2, t_k^3)$ satisfying $< \begin{pmatrix} d_{u_k}\mathcal{L}(u_k + t_k^1 d_k^1, v_k, p_k) \\ d_{v_k}\mathcal{L}(u_k, v_k + t_k^2 d_k^2, p_k) \\ d_{p_k}\mathcal{L}(u_k, v_k, p_k + t_k^3 d_k^3) \end{pmatrix}, d_k >= 0$
5. Set $u_{k+1} := u_k + t_k^1 d_k^1$ and $v_{k+1} := v_k + t_k^2 d_k^2$ and $p_{k+1} := p_k + t_k^3 d_k^3$.
6. Set $\eta_{k+1} := \begin{pmatrix} -d_{u_k}\mathcal{L}(u_{k+1}, v_k, p_k) \\ -d_{v_k}\mathcal{L}(u_k, v_{k+1}, p_k) \\ d_{p_k}\mathcal{L}(u_k, v_k, p_{k+1}) \end{pmatrix}$
7. Determine step length β_{k+1} such as: $\beta_{k+1} := \frac{<\eta_{k+1}, \eta_{k+1}>}{<\eta_k, \eta_k>}$
8. **if** $< \eta_k, d_k >\leq 0$ **then**
9. Set $d_k := \eta_k$
10. **end if**
11. **end while**

where $\otimes$ represents the Kronecker product, and the matrix D_1 represents the 1D low pass filtering given by

$$D_1 = \begin{bmatrix} 1 & 1 & 0 & 0 & \dots & 0 & 0 \\ 0 & 0 & 1 & 1 & \dots & 0 & 0 \\ \vdots & \vdots & \vdots & \vdots & \ddots & \vdots & \vdots \\ 0 & 0 & 0 & 0 & \dots & 1 & 1 \end{bmatrix}. \tag{5.2}$$

To construct the operators F_k, we used the proposed fluid registration implementation (see Algorithm 1. For that, we used bicubic upsamplings $\widehat{Y}_i$ of the LR sequence Y_i. We then selected the reference image between the upsamplings images $\widehat{Y}_i$ that is used for the super-resolution process as $\widehat{Y}_k$ $(1 \leq k \leq n)$. Through the image $\widehat{Y}_k$, we compute the optical flow to all other input images (for $i \neq k$). We get then n flow vector fields $u_i : \Omega \longrightarrow \mathbb{R}^2$. Since in the studied super-resolution model (2.1), we formulate the optical flow as a linear operator $F_i : \mathbb{R}^{r^2N^2 \times r^2N^2} \longrightarrow \mathbb{R}^{r^2N^2 \times r^2N^2}$. However, taking into account the large size of this operator $([r^2N^2 \times r^2N^2])$, its storage is difficult and also its computation is not feasible. Therefore, we use directly the fields u_i to warp the HR image with respect to the input LR images using bicubic interpolation. Finally, to compute the blurring operator H, we use a simple Gaussian kernel. The blur operator is then calculated using the kernel size 3σ, where σ is the standard deviation. We have now the necessary ingredients to implement the Algorithm 1. For the fusion step, we use the algorithm in [25, 48] to compute the blurred and noisy HR image $B = HX$. After that, we carry out the last step of the SR algorithm, which is the restoration step.

6. Restoration step

Since the problem of restoration is ill-posed, we have to be careful in the choice of a suitable approach for denoising and deconvolution step. The main purpose of this stage is to preserve image features and avoid the blocky effect while reducing noise and blur. Since first order regularizers have always suffered from the blocky effect [10], numerous approaches have been proposed to tackle this effect, namely, higher-order regularizations [8, 31, 33, 34]. Another successful approach in the super resolution framework was also proposed in [22] to preserve the details of the obtained image. A more robust higher-order total variation model is proposed as an efficient solution to the blocky effect, called total generalised variation (TGV) [44]. Even if this method avoids the

staircasing effect, the computational time to reach the solution is very significant. An alternative way is to use a combined approach of the first and second order regularizer proposed by Papafitsoros *et al.* [37] which eliminates noise and blur, avoiding the block artifacts, in less time than the TGV. In the same esprit, we introduce a first-order operator to preserve edges and a second-order one to remove noise in smooth areas. Let us describe briefly the algorithm used in the proposed SR approach. In this paper, we use the gradient descent PDE with a Neumann boundary condition on $\partial\Omega$, associated to the variational model proposed in [37]. This PDE with the initial condition $X(0,x) = X_0$ (where X_0 is the obtained HR image calculated by the interpolation of the LR image Y_1) is given by

$$\begin{cases} \partial_t X = H^\intercal \operatorname{sign}(HX - B) + \gamma \operatorname{div}\left(\frac{g_1'(|\nabla X|)}{|\nabla X|}\nabla X\right) \\ \qquad +(1-\gamma)\operatorname{div}^2\left(\frac{g_2'(\|\nabla^2 X\|)}{\|\nabla^2 X\|}\nabla^2 X\right), \\ \partial_n X = 0, \text{ on } \partial\Omega, \end{cases} \tag{6.1}$$

where the divergence operator $\operatorname{div} : (\mathbb{R}^{r^2N^2\times 1})^2 \longrightarrow \mathbb{R}^{r^2N^2\times 1}$, defined as

$$\operatorname{div} X.Y = X.\nabla Y,\ \forall X \in (\mathbb{R}^{r^2N^2\times 1})^2,\ Y \in \mathbb{R}^{r^2N^2\times 1}. \tag{6.2}$$

Also, the two divergence operator $\operatorname{div}^2 : (\mathbb{R}^{r^2N^2\times 1})^4 \longrightarrow \mathbb{R}^{r^2N^2\times 1}$, with the adjointness property, is defined

$$\operatorname{div}^2 X.Y = X.\nabla^2 Y,\ \forall X \in (\mathbb{R}^{r^2N^2\times 1})^4,\ Y \in \mathbb{R}^{r^2N^2\times 1}, \tag{6.3}$$

g_1 and g_2 are linear growth increasing functions defined: $\mathbb{R} \longrightarrow \mathbb{R}^+$, and γ : the controlled regularization parameters. The existence and uniqueness of solution to this PDE is demonstrated using the relaxation techniques [3], based on the monotony of the operators $\operatorname{div}\left(\frac{g_1'(|\nabla X|)}{|\nabla X|}\nabla X\right)$ and $\operatorname{div}^2\left(\frac{g_2'(\|\nabla^2 X\|)}{\|\nabla^2 X\|}\nabla^2 X\right)$. To solve the PDE above, we use a classical finite difference scheme.

Let $X_{i,j}$ the discrete version of the image X, such as $X_{i,j} = X(i,j)$, $i = 1 \dots M$, $j = 1 \dots M$, where $M = rN$. We give briefly the discrete version of the operators ∇ and div given by

$$(\nabla X)^1_{i,j} = \begin{cases} X_{i+1,j} - X_{i,j} & \text{if} \quad i < M \\ 0 & \text{if} \quad i = M \end{cases}, \tag{6.4}$$

$$(\nabla X)^2_{i,j} = \begin{cases} X_{i,j+1} - X_{i,j} & \text{if} \quad j < M \\ 0 & \text{if} \quad j = M \end{cases}, \tag{6.5}$$

and

$$(\operatorname{div}(p^1,p^2))_{i,j} = (\operatorname{div}(p^1,p^2))^1_{i,j} + (\operatorname{div}(p^1,p^2))^2_{i,j}, \tag{6.6}$$

where

$$(\operatorname{div}(p^1,p^2))^1_{i,j} = \begin{cases} p^1_{i,j} - p^1_{i-1,j} & \text{if} \quad 1 < i < M \\ p^1_{i,j} & \text{if} \quad i = 1 \\ 0 & \text{if} \quad i = M \end{cases}, \tag{6.7}$$

$$(\operatorname{div}(p^1,p^2))^2_{i,j} = \begin{cases} p^2_{i,j} - p^2_{i,j-1} & \text{if} \quad 1 < j < M \\ p^2_{i,j} & \text{if} \quad j = 1 \\ -p^2_{i,j-1} & \text{if} \quad j = M \end{cases}. \tag{6.8}$$

Let us define the second order discrete differential operators noted ∇^2 as

$$\nabla^2 X = \left(\nabla_{xx}X\ \nabla_{xy}X\ \nabla_{xy}X\ \nabla_{yy}X\right), \tag{6.9}$$

where

$$\nabla_{xx}X_{i,j}=\begin{cases}X_{i,M}-2X_{i,1}+X_{i,2} & \text{if } 1\le i\le M,\ j=1,\\ X_{i,j-1}-2X_{i,j}+X_{i,j+1} & \text{if } 1\le i\le M,\ 1<j<M,\\ X_{i,M-1}-2X_{i,M}+X_{i,1} & \text{if } 1\le i\le M,\ j=M,\end{cases} \tag{6.10}$$

$$\nabla_{yy}X_{i,j}=\begin{cases}X_{M,j}-2X_{1,j}+X_{2,j} & \text{if } i=1,\ 1\le j\le M,\\ X_{i-1,j}-2X_{i,j}+X_{i+1,j} & \text{if } 1<i<M,\ 1\le j\le M,\\ X_{M-1,j}-2X_{M,j}+X_{1,i} & \text{if } i=M,\ 1\le j\le M,\end{cases} \tag{6.11}$$

and

$$\nabla_{xy}X_{i,j}=\begin{cases}X_{i,j}-X_{i+1,j}-X_{i,j+1}+X_{i+1,j+1} & \text{if } 1\le i<M,\ 1\le j<M,\\ X_{i,M}-X_{i+1,M}-X_{i,1}+X_{i+1,1} & \text{if } 1\le i<M,\ j=M,\\ X_{M,j}-X_{1,j}-X_{M,j+1}+X_{1,j+1} & \text{if } i=M,\ 1\le j<M,\\ X_{M,M}-X_{1,M}-X_{M,1}+X_{1,1} & \text{if } i=M,\ j=M.\end{cases} \tag{6.12}$$

In addition, for $X=(X_1,\,X_2,\,X_3,\,X_4)\in\left(\mathbb{R}^M\right)^4$, we define the discrete div^2 operator as

$$(\mathrm{div}^2\,X)_{i,j}=\overline{\nabla_{xx}}X_{1_{i,j}}+\overline{\nabla_{yy}}X_{2_{i,j}}+\overline{\nabla_{xy}}X_{3_{i,j}}+\overline{\nabla_{xy}}X_{4_{i,j}}, \tag{6.13}$$

where

$$\overline{\nabla_{xx}}=\nabla_{xx},\ \overline{\nabla_{yy}}=\nabla_{yy}, \tag{6.14}$$

and

$$\overline{\nabla_{xy}}X_{i,j}=\begin{cases}X_{1,1}-X_{1,M_2}-X_{M_1,1}+X_{M_1,M_2} & \text{if } i=1,\ j=1,\\ X_{1,j}-X_{1,j-1}-X_{M_1,j}+X_{M_1,j-1} & \text{if } i=1,\ 1<j\le M,\\ X_{i,1}-X_{i-1,M_2}-X_{i-1,1}+X_{i-1,M_2} & \text{if } 1<i\le M,\ j=1,\\ X_{i,j}-X_{i,j-1}-X_{i-1,j}+X_{i-1,j-1} & \text{if } 1<i\le M,\ 1<j\le M.\end{cases} \tag{6.15}$$

To give a comprehensive form of this problem, we set the particular case where $g_1(x)=g_2(x)=x$. As a result, the algorithm related to solve numerically the proposed PDE is finally given in **Algorithm 1**.

Algorithm 2 The proposed algorithm.

Inputs: The blurred image B; the steepest descent parameter $\mathrm{d}t$. the regularization parameter γ.
To avoid the derivative singularity when X is locally constant (in the special case where the denominator is equal to zero), we introduce a small parameter $\epsilon>0$;
The procedure:

$$\begin{aligned}\widehat{X}_{i,j}^{n+1}=\widehat{X}_{i,j}^{n}&+dt\big(H_{i,j}^{\intercal}\mathrm{sing}((H\widehat{X})_{i,j}^{n}-B_{i,j})\big)+dt\gamma\ \mathrm{div}_{i,j}^{1}\left(\frac{(\nabla\widehat{X})_{i,j}^{1}}{\sqrt{((\nabla\widehat{X})_{i,j}^{1})^2+((\nabla\widehat{X})_{i,j}^{2})^2+\epsilon}}\right)\\&+dt\gamma\ \mathrm{div}_{i,j}^{2}\left(\frac{(\nabla\widehat{X})_{i,j}^{2}}{\sqrt{((\nabla\widehat{X})_{i,j}^{1})^2+((\nabla\widehat{X})_{i,j}^{2})^2+\epsilon}}\right)\\&+dt\,(1-\gamma)\,\overline{\nabla_{xx}}\left(\frac{\nabla_{xx}\widehat{X}_{i,j}^{n}}{\sqrt{1+(\nabla_{xx}\widehat{X}_{i,j}^{n})^2+(\nabla_{yy}\widehat{X}_{i,j}^{n})^2+2(\nabla_{xy}\widehat{X}_{i,j}^{n})^2}}\right)\\&+dt\,(1-\gamma)\,\overline{\nabla_{yy}}\left(\frac{\nabla_{yy}\widehat{X}_{i,j}^{n}}{\sqrt{1+(\nabla_{xx}\widehat{X}_{i,j}^{n})^2+(\nabla_{yy}\widehat{X}_{i,j}^{n})^2+2(\nabla_{xy}\widehat{X}_{i,j}^{n})^2}}\right)\\&+2\,dt\,(1-\gamma)\,\overline{\nabla_{xy}}\left(\frac{\nabla_{xy}\widehat{X}_{i,j}^{n}}{\sqrt{1+(\nabla_{xx}\widehat{X}_{i,j}^{n})^2+(\nabla_{yy}\widehat{X}_{i,j}^{n})^2+2(\nabla_{xy}\widehat{X}_{i,j}^{n})^2}}\right)\quad i,j=1,\ldots,M\end{aligned}$$

Output: The restored HR image $\widehat{X}$

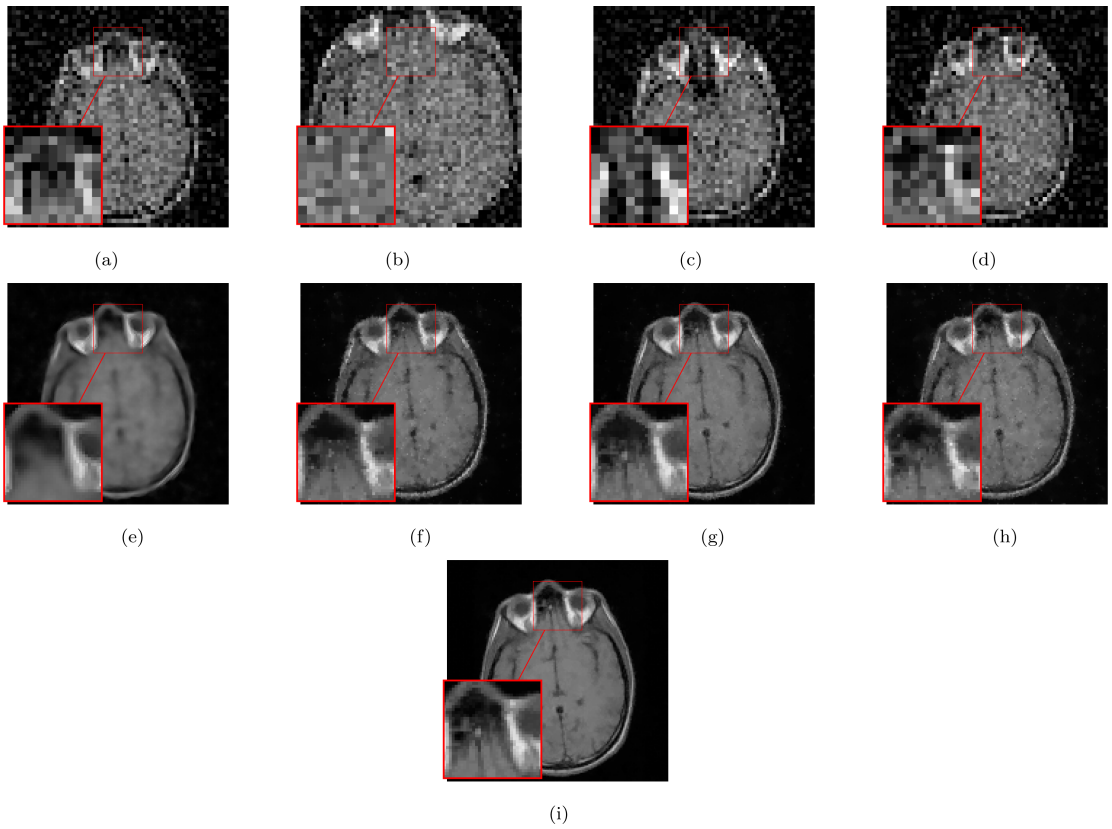

FIGURE 1. Comparisons of different SR methods with different registration procedure of the (*MRI brain 1* image when the magnification factor is $r = 3$ using random motion vectors) to perform the registration step. Note that the noise is considered with a standard deviation $\sigma = 35$. (a) First LR image. (b) 16th LR image. (c) 18th LR image. (d) 32th LR image. (e) POF [16]. (f) SRCF [51]. (g) SRHE [29]. (h) SRDR [25]. (i) Our method.

7. EXPERIMENTS

In this part, our aim is to test the ability of the elaborated algorithm in the SR context. Many simulated and also real results were used to test the performance of the proposed SR method. The first part is dedicated to the evaluation of the registration part while the second and third parts concern the main proposed SR approach.

7.1. The effectiveness of the registration part

In the first experience, we construct 32 synthetic LR images from the original image of *MRI Brain 1* such that: each frame is deformed by random vector fields, blurred by a Gaussian low-pass filter with size 4×4 and a standard deviation of 2. Then the blurred frames are down-sampled in the two directions by a factor of $r = 3$ and a Gaussian noise was added with a standard deviation $\sigma = 20$. In this test, we fix the deconvolution and denoising part where we use the proposed combined first and second order regularizer. Then, we compare our registration algorithm with other competitive registration methods in the SR context, such as: SR with probabilistic optical flow (POF) [16], SR with hyper-elastic (SRHE) [29], SR with consistent flow (SRCF) [51] and also SR with diffusion registration (SRDR) proposed in [25]. The obtained SR results are shown in Figure 1 to see the efficiency of the proposed registration part. We can deduce that the proposed registration method

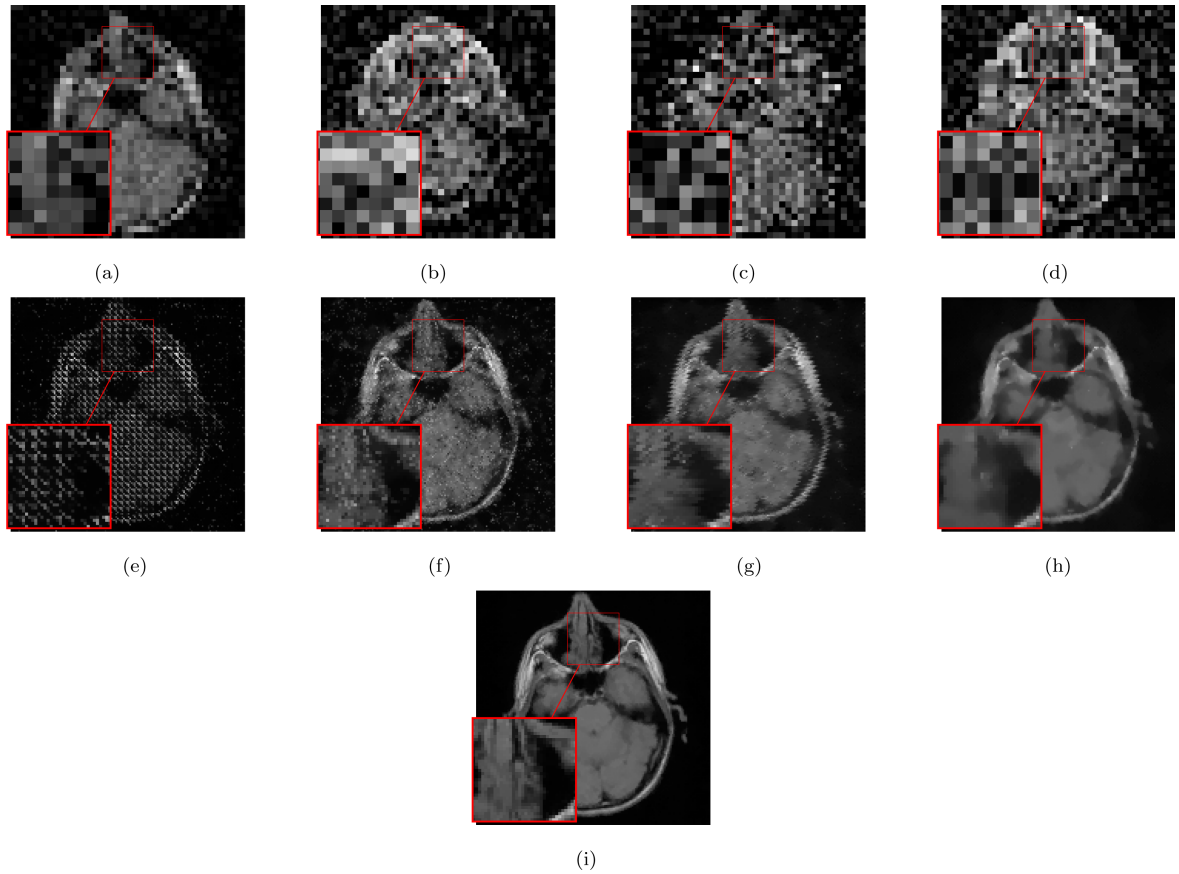

FIGURE 2. Comparisons of different SR methods with different registration procedure of the (*MRI brain 2* image when the magnification factor is $r = 3$ using random motion vectors) to perform the registration step. Note that the noise is considered with a standard deviation $\sigma = 35$. (a) First LR image. (b) 16th LR image. (c) 18th LR image. (d) 32th LR image. (e) POF [16]. (f) SRCF [51]. (g) SRHE [29]. (h) SRDR [25]. (i) Our method.

gives a slightly better result compared to the other methods. For the second experiment, we consider the *MRI Brain 1* following the same previous steps with more complicated random deformations between the LR images. We increase also the decimation factor $r = 4$ and also the standard deviation $\sigma = 35$. The obtained HR image is depicted in Figure 2, where comparison to other SR methods is done. Clearly the obtained HR image outperforms the other ones and the registration process is better enhanced.

In the following tests, the first six experiments were simulated ones with known HR images, while the next three experiments were real data experiments. In all simulated experiments, we measure the effectiveness of our method by considering some comparisons with popular SR methods, such as bicubic interpolation, BTV [15], $SWTV$ SR method [49] and also the combined first order and BTV ($TV + BTV$) regularisation [24] using the same data. In the following experiments, the motion model is assumed to be the global translational model for the other methods while we use the fluid registration for our approach. In this paper, in the simulated experiments, the peak-signal-to-noise ratio (PSNR) [21] and also the structural similarity (SSIM) [45] are computed to check the quality of the recovered HR image.

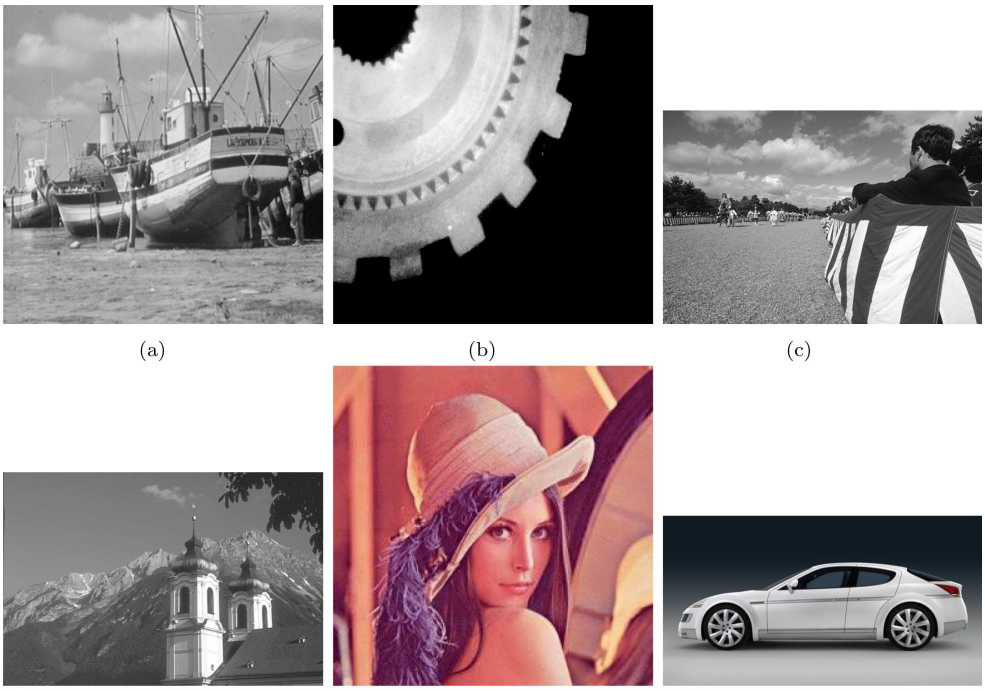

FIGURE 3. The original six images used in simulated tests. (a) Boat. (b) Gear. (c) Festival. (d) Mosq. (e) Lena. (f) Car.

7.2. Simulated Experiments

In the simulated experiments, we choose six examples in Figure 3, with different size and texture, taken from a tested benchmark images to illustrate the performance of the proposed SR method. To construct the simulated images, we follow the degradation model (2.1). The HR image was first shifted with sub-pixel displacements to produce N images, then, the sequence was convoluted with a PSF and finally, zero-mean Gaussian noise was added to each frame of the sequence. For example, in the first experiment, we take the image of *Boat* 3a as an original image of size 512×512, we construct then $N = 50$ input low-resolution frames by shifting the Figure 3a in vertical and horizontal directions, sub-sampling with a decimation factor $r = 4$ and blurred using a Gaussian density with kernel size 3×2. Finally, we add a white Gaussian noise e_k in each frame with a standard deviation $\sigma = 10$. We use the same thing for the *Gear* image, while we increase the blur kernel rate and σ noise for the other tests. Indeed, we use a 5×5 Gaussian blur kernel and a white Gaussian noise with $\sigma = 30$ to construct the sequence for the last four images. To increase the ability of the proposed equation to better detect edges, we choose the so-called hypersurface minimal function [3] defined for both the functions g_1 and g_2 by

$$g_1(x) = g_2(x) = \sqrt{1 + x^2}. \tag{7.1}$$

The input HR image X^0 is built by a bicubic interpolation of the LR reference image Y_1. Concerning the choice of the parameters, the scalar weight γ is chosen according to the better PSNR value for the proposed and also for the other SR methods. For instance, we choose $\gamma = 0.6$ for *the Boat* image. Concerning the convergence of the proposed algorithm, we end the execution at the first iteration n with respect to the error $\dfrac{\|\widehat{X}^{n+1} - \widehat{X}^n\|_1}{\|\widehat{X}^n\|_1} < 10^{-5}$. We set also $\epsilon = 10^{-3}$.

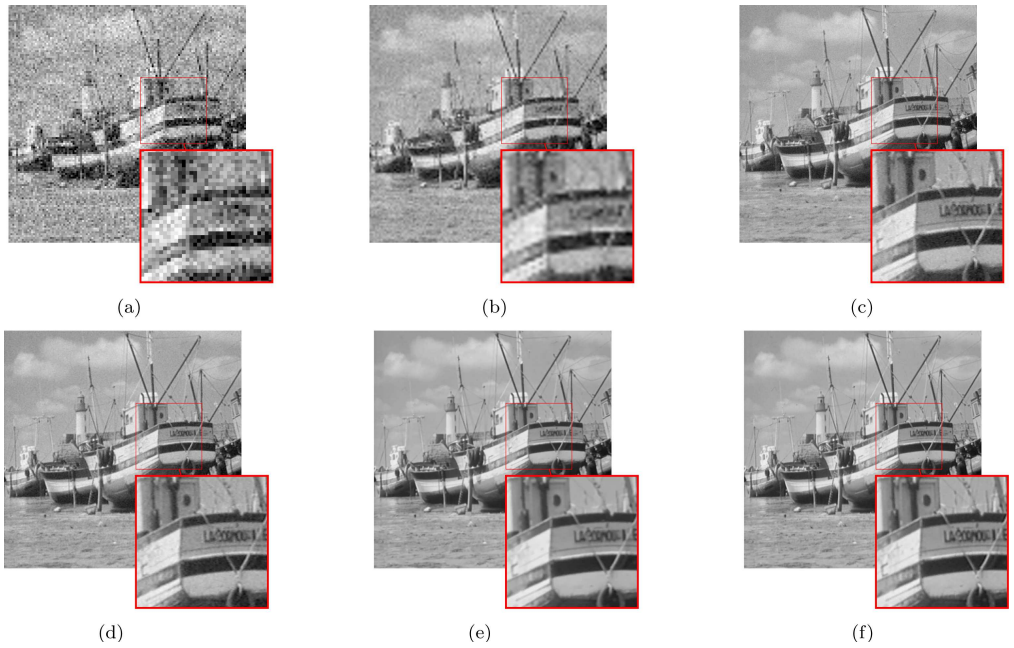

FIGURE 4. Super resolution of *the Boat* compared with different methods. (a) One LR image. (b) Bicubic zoom. (c) BTV reg. [15]. (d) $SWTV$ method [49]. (e) $TV + BTV$ reg. [24]. (f) The proposed SR.

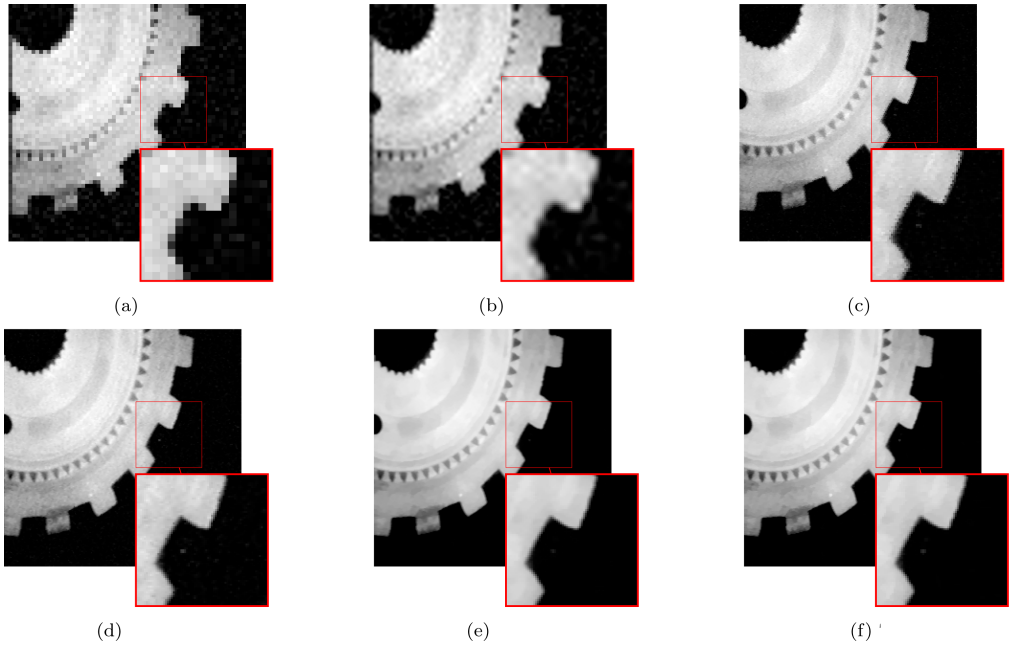

FIGURE 5. Super resolution of *the Gear* compared with different methods. (a) One LR image. (b) Bicubic zoom. (c) BTV reg. [15]. (d) $SWTV$ method [49]. (e) $TV + BTV$ reg. [24]. (f) The proposed SR.

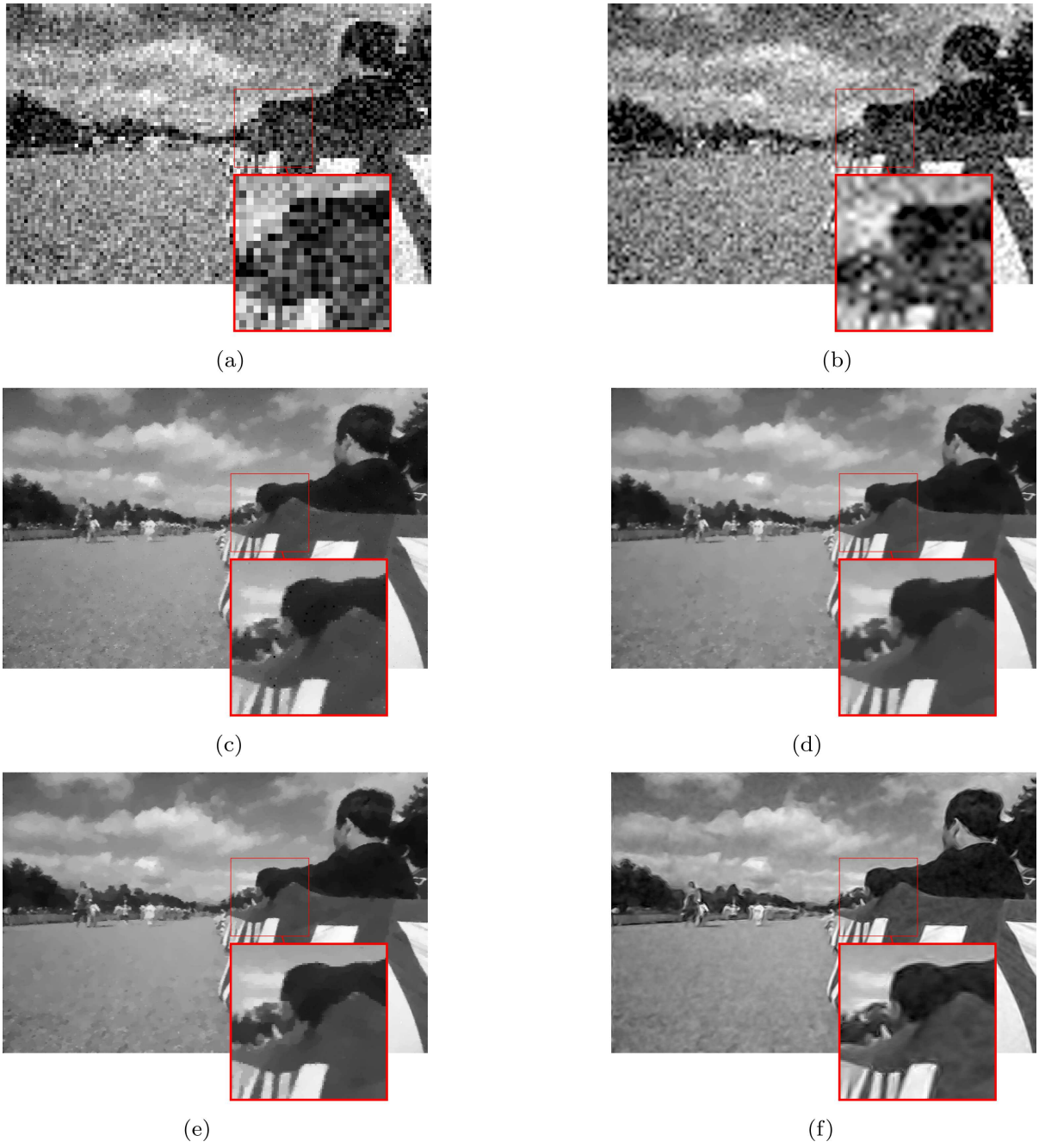

FIGURE 6. Super resolution of *Festival* compared with different methods. (a) One LR image. (b) Bicubic zoom. (c) BTV reg. [15]. (d) $SWTV$ method [49]. (e) $TV + BTV$ reg. [24]. (f) The proposed SR.

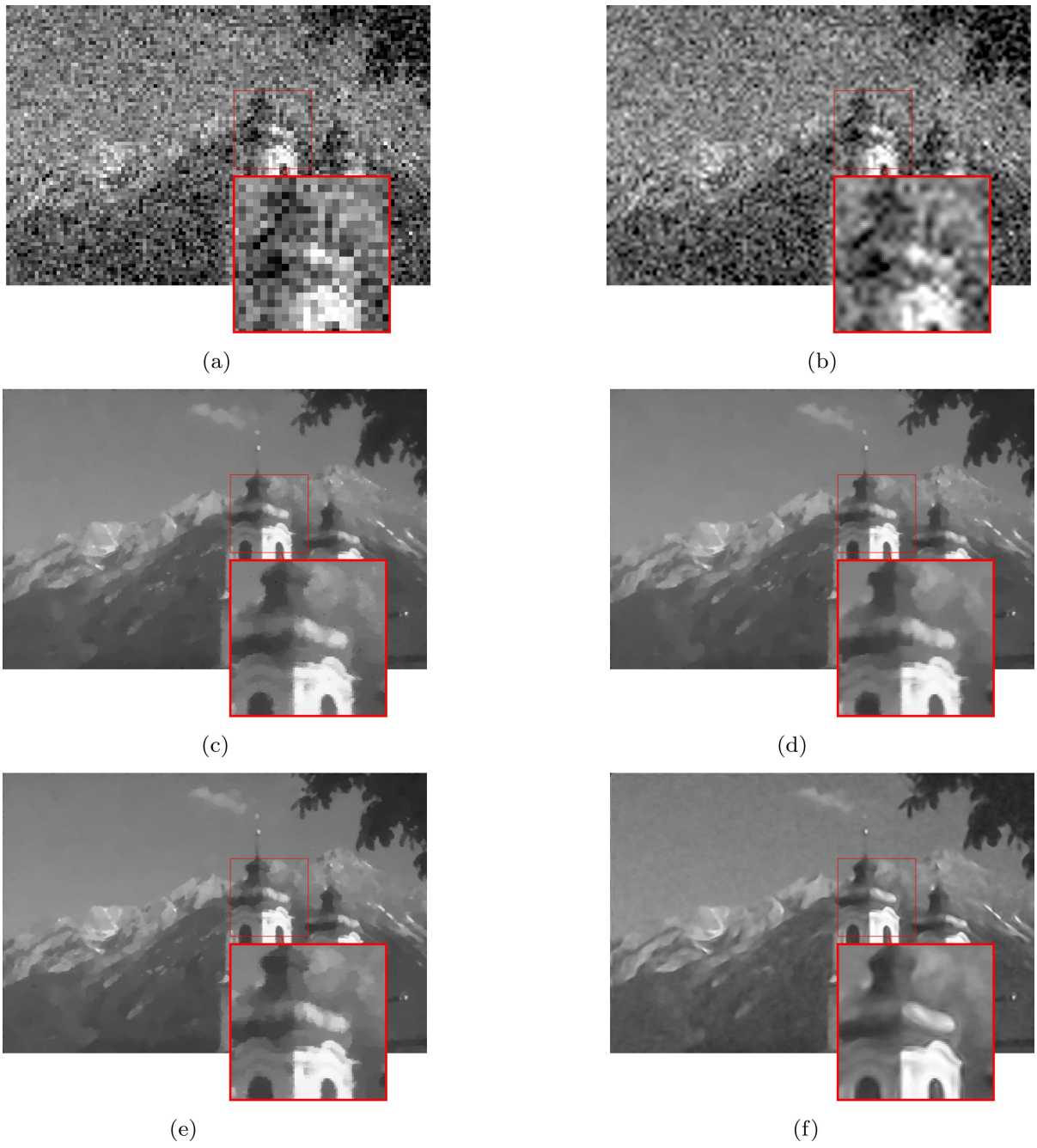

FIGURE 7. Super resolution of *Mosq* compared with different methods. (a) One LR image. (b) Bicubic zoom. (c) BTV reg. [15]. (d) $SWTV$ method [49]. (e) $TV + BTV$ reg. [24]. (f) The proposed SR.

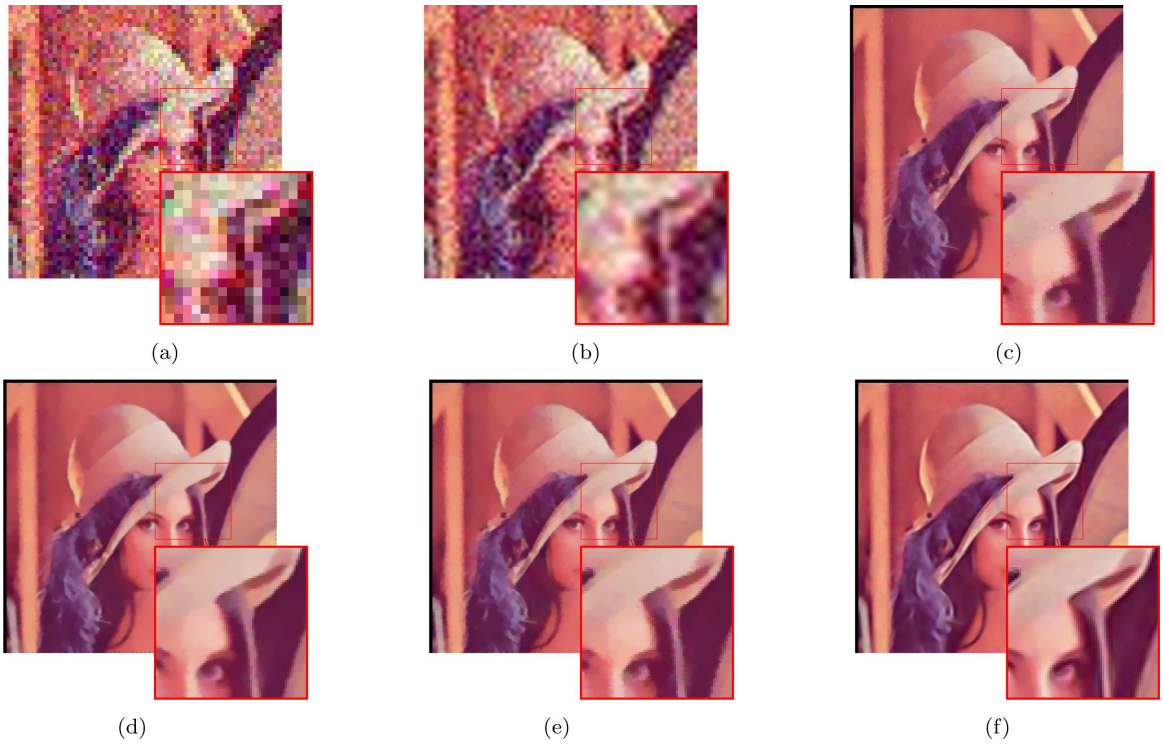

FIGURE 8. Super resolution of *Lena* compared with different methods. (a) One LR image. (b) Bicubic zoom. (c) BTV reg. [15]. (d) $SWTV$ method [49]. (e) $TV + BTV$ reg. [24]. (f) The proposed SR.

The obtained results using the proposed SR are illustrated and compared with other approaches in the Figures 4–9 for the tested image in Figure 3 respectively. Visually, we can see that the proposed model gives better restoration than the others. The difference becomes more obvious when the σ noise and blur increase which is the case in the Figures 6–9. The effectiveness of the proposed approach model can also be shown in the color images in Figures 8 and 9, where the obtained HR image is more clean with fewer registration errors. However, to approve the success of the proposed algorithm against noise and misregistration errors reducing, we use the PSNR criterion in the Table 1 and the SSIM measure in the Table 2 for three σ noise values. Knowing that the best score is in bold number, we can clearly show the efficiency of our algorithm. Also, visually, we can detect the performance of the proposed method in removing misregistration errors compared with the other methods in the smooth area, however, in the edge area there is no distinct improvement compared to $TV+BTV$ and $SWTV$ methods.

7.3. Real Experiments

In the real experiments, three real data sequences are used to approve the proposed algorithm, are presented. We select the first ten frames in the three real data sets. The registration approach presented in [44] is used as the registration estimation method for the other methods while we use the proposed fluid registration to estimate the motion for our method. The reconstruction results of these sequences are, respectively, shown in Figures 10–12. From these figures, it is shown that the proposed approach gives a better visual effect compared to the other method.

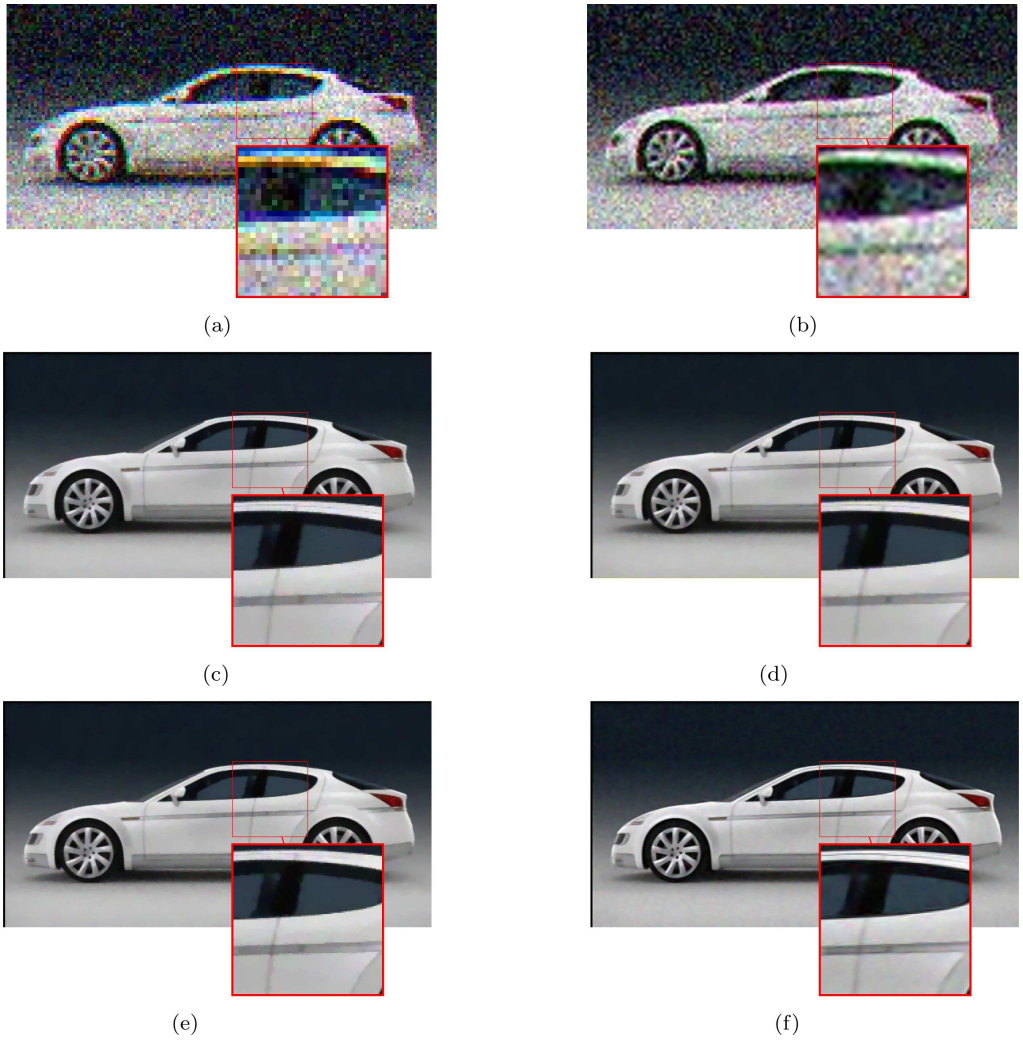

FIGURE 9. Super resolution of *Car* compared with different methods. (a) One LR image. (b) Bicubic zoom. (c) *BTV* reg. [15]. (d) *SWTV* method [49]. (e) $TV + BTV$ reg. [24]. (f) The proposed SR.

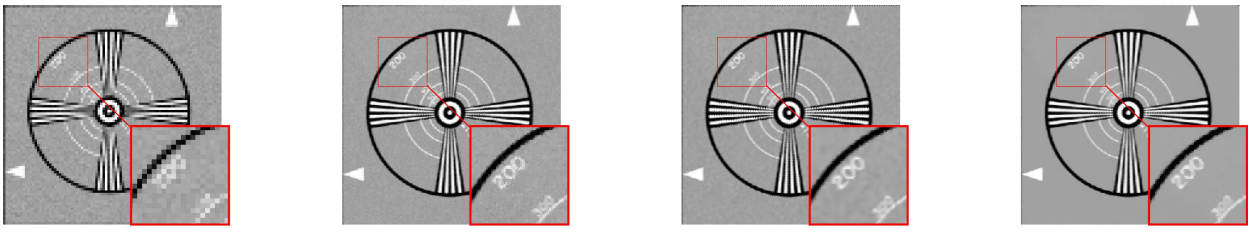

FIGURE 10. Results on the *EIA* sequence. (a) First LR frame. (b) $TV + BTV$ reg. [24]. (c) *SWTV* method [49]. (d) Our method.

TABLE 1. The PSNR table.

Image	Method	$\sigma = 10$	$\sigma = 20$	$\sigma = 30$
Boat	Bicubic interpolation	21.46	20.02	19.88
	BTV [15]	28.93	27.89	27.03
	SWTV [49]	29.53	28.78	28.01
	$TV + BTV$ [24]	29.58	28.76	27.84
	The Proposed approach	**30.41**	**29.92**	**29.13**
Gear	Bicubic interpolation	18.49	17.66	19.98
	BTV [15]	31.98	31.22	30.87
	SWTV [49]	33.50	33.18	32.81
	$TV + BTV$ [24]	34.08	33.59	32.41
	The Proposed approach	**35.41**	**35.02**	**34.55**
Festival	Bicubic interpolation	19.01	18.22	17.36
	BTV [15]	31.22	30.89	30.14
	SWTV [49]	32.02	31.12	30.77
	$TV + BTV$ [24]	32.08	31.72	31.06
	The Proposed approach	**33.15**	**32.87**	**32.24**
Mosq	Bicubic interpolation	19.96	19.06	18.71
	BTV [15]	30.22	29.72	29.08
	SWTV [49]	31.53	31.01	30.74
	$TV + BTV$ [24]	31.18	30.69	30.02
	The Proposed approach	**32.88**	**32.42**	**32.01**
Lena	Bicubic interpolation	21.06	20.68	20.03
	BTV [15]	31.22	30.95	30.18
	SWTV [49]	32.44	32.02	31.75
	$TV + BTV$ [24]	32.34	32.04	31.71
	The Proposed approach	**33.01**	**32.88**	**32.62**
Car	Bicubic interpolation	19.22	18.85	18.12
	BTV [15]	29.66	29.15	28.76
	SWTV [49]	30.99	30.75	30.36
	$TV + BTV$ [24]	31.03	30.76	30.22
	The Proposed approach	**32.14**	**31.89**	**31.46**

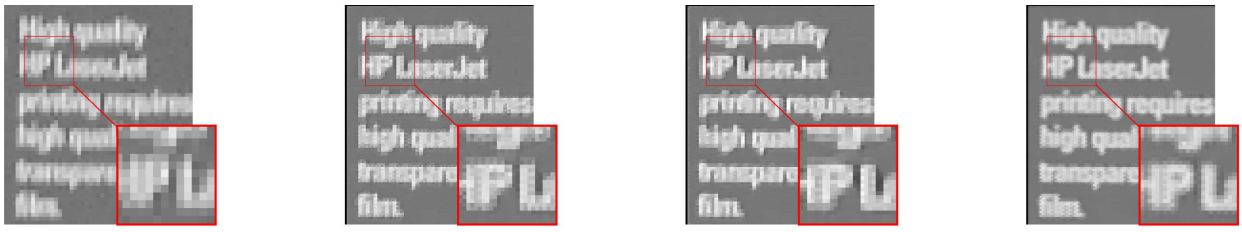

(a) (b) (c) (d)

FIGURE 11. Results on the *Text* sequence. (a) First LR frame. (b) $TV + BTV$ reg. [24]. (c) *SWTV* method [49]. (d) Our method.

TABLE 2. The SSIM table.

Image	Method	$\sigma = 10$	$\sigma = 20$	$\sigma = 30$
Boat	Bicubic interpolation	0.591	0.538	0.499
	BTV [15]	0.822	0.795	0.748
	SWTV [49]	0.866	0.835	0.806
	$TV + BTV$ [24]	0.861	0.830	0.809
	The Proposed approach	**0.921**	**0.895**	**0.863**
Gear	Bicubic interpolation	0.602	0.581	0.521
	BTV [15]	0.851	0.801	0.788
	SWTV [49]	0.903	0.879	0.838
	$TV + BTV$ [24]	0.917	0.889	0.840
	The Proposed approach	**0.959**	**0.919**	**0.894**
Festival	Bicubic interpolation	0.685	0.638	0.601
	BTV [15]	0.877	0.839	0.808
	SWTV [49]	0.927	0.899	0.875
	$TV + BTV$ [24]	0.923	0.897	0.870
	The Proposed approach	**0.968**	**0.931**	**0.908**
Mosq	Bicubic interpolation	0.607	0.591	0.542
	BTV [15]	0.811	0.782	0.755
	SWTV [49]	0.863	0.840	0.817
	$TV + BTV$ [24]	0.853	0.835	0.816
	The Proposed approach	**0.888**	**0.859**	**0.835**
Lena	Bicubic interpolation	0.679	0.626	0.598
	BTV [15]	0.869	0.841	0.813
	SWTV [49]	0.893	0.871	0.844
	$TV + BTV$ [24]	0.896	0.877	0.842
	The Proposed approach	**0.918**	**0.898**	**0.871**
Car	Bicubic interpolation	0.603	0.582	0.553
	BTV [15]	0.802	0.786	0.742
	SWTV [49]	0.851	0.818	0.803
	$TV + BTV$ [24]	0.856	0.811	0.799
	The Proposed approach	**0.911**	**0.885**	**0.829**

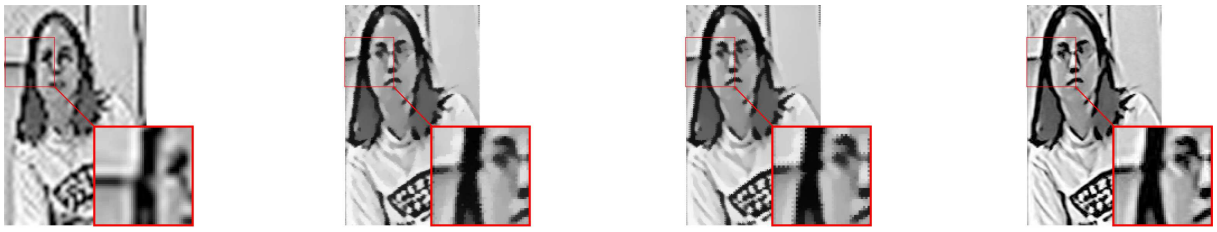

(a) (b) (c) (d)

FIGURE 12. Results on the *Emily* sequence. (a) First LR frame. (b) $TV + BTV$ reg. [24]. (c) *SWTV* method [49]. (d) Our method.

8. Conclusion

In this paper, a novel approach of the super resolution image reconstruction problem is introduced. We presented a bilevel fluid image registration and proved the existence and uniqueness of the solution using functional analysis theory. In addition, to avoid the undesirable staircasing effect during the registration, denoising and deconvolution steps, a fourth-order PDE is proposed. To show the robustness of this approach, a set of benchmark image have been performed, and the investigated SR approach has proven its success visually and also quantitatively using two known metrics. A remaining question is about the treatment of other types of noise and blur, such as Salt& paper and Poisson noise. Another interesting point is about the degrees of the efficiency of the proposed approach with respect to the nature of the transformations between the LR frames.

Acknowledgements. The authors are very grateful to the reviewers for their suggestions and corrections.
Conflict of interest. The authors have no conflict of interest.

References

[1] M. Alahyane, A. Hakim, A. Laghrib and S. Raghay, A fast approach of nonparametric elastic image registration problem. *Math. Methods Appl. Sci.* **42** (2019) 7059–7075.
[2] J.P Ardila, V.A. Tolpekin, W. Bijker and A. Stein, Markov-random-field-based super-resolution mapping for identification of urban trees in vhr images. *ISPRS J. Photogramm. Remote Sens.* **66** (2011) 762–775.
[3] G. Aubert and P. Kornprobst, Mathematical problems in image processing: partial differential equations and the calculus of variations, Vol. 147. Springer Science & Business Media (2006).
[4] J.P. Aubin, Un théorème de compacité. *Acad. Sci. Paris* **256** (1963) 5042–5044.
[5] R.M. Bahy, G.I. Salama and T.A. Mahmoud, Adaptive regularization-based super resolution reconstruction technique for multi-focus low-resolution images. *Signal Process.* **103** (2014) 155–167.
[6] S. Baker and T. Kanade. Super-resolution optical flow. Carnegie Mellon University, The Robotics Institute (1999).
[7] S. Baker and T. Kanade, Limits on super-resolution and how to break them. *IEEE Trans. Pattern Anal. Mach. Intell.* **24** (2002) 1167–1183.
[8] M. Bergounioux and L. Piffet, A second-order model for image denoising. *Set-Valued Var. Anal.* **18** (2014) 277–306.
[9] H. Brezis, Functional Analysis, Sobolev Spaces and Partial Differential Equations. Springer (2011).
[10] A. Buades, B. Coll and J.-M. Morel, The staircasing effect in neighborhood filters and its solution. *IEEE Trans. Image Process.* **15** (2006) 1499–1505.
[11] A. Chambolle and P.-L. Lions, Image recovery via total variation minimization and related problems. *Numer. Math.* **76** (1997) 167–188.
[12] F. Demengel and G. Demengel, Espaces fonctionnels. Utilisation dans la résolution des équations aux dérivées partielles. CNRS Editions (2007).
[13] I. El Mourabit, M. El Rhabi, A. Hakim, A. Laghrib and E. Moreau, A new denoising model for multi-frame super-resolution image reconstruction. *Signal Process.* **132** (2017) 51–65.
[14] I. El Mourabit, A. Hakim and A. Laghrib, An anisotropic pde for multi-frame super-resolution image reconstruction. In International Conference on Numerical Analysis and Optimization Days. Springer (2021) 29–41.
[15] S. Farsiu, M.D. Robinson, M. Elad and P. Milanfar, Fast and robust multiframe super resolution. *IEEE Trans. Image Process.* **13** (2004) 1327–1344.
[16] R. Fransens, C. Strecha and L. Van Gool, Optical flow based super-resolution: A probabilistic approach. *Comput. Vis. Image Underst.* **106** (2007) 106–115.
[17] D. Ghosh, N. Kaabouch and W.-C. Hu, A robust iterative super-resolution mosaicking algorithm using an adaptive and directional huber-markov regularization. *J. Vis. Commun. Image Represent.* **40** (2016) 98–110.
[18] H. Greenspan, G. Oz, N. Kiryati and S.L.B.G. Peled, Mri inter-slice reconstruction using super-resolution. *Magn. Reson. Imaging* **20** (2002) 437–446.
[19] Y. Han, C. Xu, G. Baciu and X. Feng, Multiplicative noise removal combining a total variation regularizer and a nonconvex regularizer. *Int. J. Comput. Math.* **91** (2014) 2243–2259.
[20] Y. He, K.-H. Yap, L. Chen and L.-P. Chau, A nonlinear least square technique for simultaneous image registration and super-resolution. *IEEE Trans. Image Process.* **16** (2007) 2830–2841.
[21] Q. Huynh-Thu and M. Ghanbari, Scope of validity of psnr in image/video quality assessment. *Electron. Lett.* **44** (2008) 800–801.
[22] M. Jung, A. Marquina and L.A. Vese, Variational multiframe restoration of images degraded by noisy (stochastic) blur kernels. *J. Comput. Appl. Math.* **240** (2013) 123–134.

[23] N. Kumar, R. Verma and A. Sethi, Convolutional neural networks for wavelet domain super resolution. *Pattern Recognit. Lett.* **90** (2017) 65–71.

[24] A. Laghrib, A. Hakim and S. Raghay, A combined total variation and bilateral filter approach for image robust super resolution. *EURASIP J. Image Video Process.* **2015** (2015) 1–10.

[25] A. Laghrib, A. Ghazdali, A. Hakim and S. Raghay, A multi-frame super-resolution using diffusion registration and a nonlocal variational image restoration. *Comput. Math. Appl.* **72** (2016) 2535–2548.

[26] A. Laghrib, A. Ben-Loghfyry, A. Hadri and A. Hakim, A nonconvex fractional order variational model for multi-frame image super-resolution. *Signal Process. Image Commun.* **67** (2018) 1–11.

[27] A. Laghrib, M. Ezzaki, M. El Rhabi, A. Hakim, P. Monasse and S. Raghay, Simultaneous deconvolution and denoising using a second order variational approach applied to image super resolution. *Comput. Vis. Image Underst.* **168** (2018) 50–63.

[28] A. Laghrib, A. Hadri and A. Hakim, An edge preserving high-order pde for multiframe image super-resolution. *J. Franklin Inst.* **356** (2019) 5834–5857.

[29] A. Laghrib, A. Hadri, A. Hakim and S. Raghay, A new multiframe super-resolution based on nonlinear registration and a spatially weighted regularization. *Inf. Sci.* **493** (2019) 34–56.

[30] A. Laghrib, A. Chakib, A. Hadri and A. Hakim, A nonlinear fourth-order pde for multi-frame image super-resolution enhancement. *Discrete Contin. Dyn. Syst.-B* **25** (2020) 415.

[31] R. Lai, X.-C. Tai and T.F. Chan, A ridge and corner preserving model for surface restoration. *SIAM J. Sci. Comput.* **35** (2013) A675–A695.

[32] L.F. Lang, S. Neumayer, O. Öktem and C.-B. Schönlieb, Template-based image reconstruction from sparse tomographic data. *Appl. Math. Optim.* (2019) 1–29.

[33] S. Lefkimmiatis, A. Bourquard and M. Unser, Hessian-based norm regularization for image restoration with biomedical applications. *IEEE Trans. Image Process.* **21** (2012) 983–995.

[34] M. Lysaker and X.-C. Tai, Iterative image restoration combining total variation minimization and a second-order functional. *Int. J. Comput. Vis.* **66** (2006) 5–18.

[35] B.J. Maiseli, N. Ally and H. Gao, A noise-suppressing and edge-preserving multiframe super-resolution image reconstruction method. *Signal Process. Image Commun.* **34** (2015) 1–13.

[36] J. Modersitzki, Numerical Methods for Image Registration. Oxford University Press, USA (2007).

[37] K. Papafitsoros and C.-B. Schönlieb, A combined first and second order variational approach for image reconstruction. *J. Math. Imaging Vis.* **48** (2014) 308–338.

[38] M.K. Park and M.G. Kang, Regularized high-resolution reconstruction considering inaccurate motion information. *Opt. Eng.* **46** (2007) 117004.

[39] M. Protter, M. Elad, H. Takeda and P. Milanfar, Generalizing the nonlocal-means to super-resolution reconstruction. *IEEE Trans. Image Process.* **18** (2008) 36–51.

[40] P. Rasti, H. Demirel and G. Anbarjafari, Improved iterative back projection for video super-resolution. In 2014 22nd Signal Processing and Communications Applications Conference (SIU). IEEE (2014) 552–555.

[41] M.D. Robinson, S.J. Chiu, C.A. Toth, J.A. Izatt, J.Y. Lo and S. Farsiu, New applications of super-resolution in medical imaging. In *Super-Resolution Imaging*. CRC Press (2017) 401–430.

[42] D.A. Sorrentino and A. Antoniou, Storage-efficient quasi-newton algorithms for image super-resolution. In 2009 16th International Conference on Digital Signal Processing. IEEE (2009) 1–6.

[43] H. Su, N. Jiang, Y. Wu and J. Zhou, Single image super-resolution based on space structure learning. *Pattern Recognit. Lett.* **34** (2013) 2094–2101.

[44] T. Valkonen, K. Bredies and F. Knoll, Total generalized variation in diffusion tensor imaging. *SIAM J. Imaging Sci.* **6** (2013) 487–525.

[45] Z. Wang, A.C. Bovik, H.R. Sheikh and E.P. Simoncelli, Image quality assessment: from error visibility to structural similarity. *IEEE Trans. Image Process.* **13** (2004) 600–612.

[46] F.W. Wheeler, R.T. Hoctor and E.B. Barrett, Super-resolution image synthesis using projections onto convex sets in the frequency domain. In Vol. 5674 of Computational Imaging III. International Society for Optics and Photonics (2005) 479–490.

[47] S. Yang, M. Wang, Y. Sun, F. Sun and L. Jiao, Compressive sampling based single-image super-resolution reconstruction by dual-sparsity and non-local similarity regularizer. *Pattern Recognit. Lett.* **33** (2012) 1049–1059.

[48] X. Yang and J. Yang, Efficient diffeomorphic metric image registration via stationary velocity. *J. Comput. Sci.* **30** (2019) 90–97.

[49] Q. Yuan, L. Zhang and H. Shen, Multiframe super-resolution employing a spatially weighted total variation model. *IEEE Trans. Circuits Syst. Video Technol.* **22** (2012) 379–392.

[50] L. Yue, H. Shen, J. Li, Q. Yuan, H. Zhang and L. Zhang, Image super-resolution: The techniques, applications, and future. *Signal Process.* **128** (2016) 389–408.

[51] W. Zhao, H. Sawhney, M. Hansen and S. Samarasekera, Super-fusion: a super-resolution method based on fusion. In Vol. 2 of Object recognition supported by user interaction for service robots. IEEE (2002) 269–272.